高性能电容器用富勒烯/石墨烯三维全碳杂化材料

程 蕾[1]， 李幸娟[1]， 李 静[1]， 邱汉迅[1]， 薛裕华[1]， Kuznetsova-Iren Evgenyevna[2]，
Vladimir Kolesov[2]， 陈成猛[3]， 杨俊和[1]

（1. 上海理工大学 材料科学与工程学院，上海 200093；
2. Kotelnikov Institute of Radio Engineering and Electronics，
Russian Academy of Science，Moscow 125009，Russia；
3. 中国科学院山西煤化学研究所 炭材料重点实验室，山西 太原 030001）

摘 要： 通过简单的水热过程将C_{60}分子引入石墨烯片层，可控制备了具有三维多孔结构的全碳C_{60}/石墨烯杂化材料，该材料作电极材料时电容性能得到明显提高。研究表明，C_{60}分子和石墨烯骨架中的碳六元环之间的共轭相互作用有利于C_{60}与石墨烯在高压水热条件下自组装形成三维多孔结构。C_{60}分子的加入使杂化产物具有优化的多孔结构和更多的氧化还原活性位点，这赋予杂化产物优异的电化学性能。以浓度为6 mol/L KOH溶液作为电解质，当电流密度为1 A/g时，其比电容为332.3 F/g，与三维多孔结构石墨烯材料电极相比提高了54.5%。此外，作为完全由碳原子组成的复合电极材料，其表现出的电化学性能优于文献报道的类似碳基材料。这一研究表明全碳杂化电极材料在用于制造高性能超级电容器方面具有很强竞争力和广阔应用前景，为未来基于全碳电极的高性能储能器件的设计和制备提供了有价值参考。

关键词： 石墨烯；富勒烯（C_{60}）；全碳杂化；电化学性能；超级电容器

中图分类号： TB33 **文献标识码：** A

基金项目：上海市自然科学基金（18ZR1426300，17511101603）；上海市教委创新重点项目（2019-01-07-00-07-E00015）；俄罗斯基础研究基金（18-29-23042）.

通讯作者：邱汉迅，副教授. E-mail：hxqiu@usst.edu.cn

作者简介：程 蕾，硕士研究生. E-mail：ryoma0401@126.com

Construction of three-dimensional all-carbon C_{60}/graphene hybrids and their use as electrodes for high performance supercapacitors

CHENG Lei[1]， LI Xing-juan[1]， LI Jing[1]， QIU Han-xun[1]，XUE Yu-hua[1]， Kuznetsova-Iren Evgenyevna[2]
Vladimir Kolesov[2]， CHEN Cheng-meng[3]， YANG Jun-he[1]

（1. *School of Materials Science and Engineering*，*University of Shanghai for Science and Technology*，*Shanghai* 200093，*China*；
2. *Kotelnikov Institute of Radio Engineering and Electronics*，*Russian Academy of Science*，*Moscow* 125009，*Russia*；
3. *CAS Key Laboratory of Carbon Materials*，*Institute of Coal Chemistry*，*Chinese Academy of Sciences*，*Taiyuan* 030001，*China*）

Abstract： Control of the three-dimensional（3D）pore structure of all-carbon C_{60}/graphene hybrids was conducted by introducing C_{60} molecules into graphene laminates by a simple hydrothermal method to improve their performance as electrodes in supercapacitors. Results indicate that the strong π-π interaction between carbon hexagons in C_{60} and graphene skeletons favors the self-assembly of the 3D pore structure of the C_{60}/graphene hybrids under hydrothermal conditions. The addition of C_{60} molecules gives the hybrids a hierarchical pore structure and redox-active sites，which contribute remarkably to the improved electrochemical performance. A specific capacitance of 332.3 $F\cdot g^{-1}$ at a current density of 1 $A\cdot g^{-1}$ was obtained in a 6 $mol\cdot L^{-1}$ potassium hydroxide solution for a hybrid optimized by an orthogonal experimental design method，which is 54.5% higher than that of the graphene without C_{60}. This finding indicates that the all-carbon hybrids may be used as more competitive and promising electrodes for the fabrication of high performance supercapacitors.

Key words： Graphene；C_{60}；All-carbon hybrid；Electrochemical performance；Supercapacitors

Received date：2020-03-26； *Revised date*：2020-11-11

Foundation items：Science and Technology Commission of Shanghai Municipality（18ZR1426300，17511101603），Innovation Program of Shanghai Municipal Education Commission（2019-01-07-00-07-E00015）and Russian Foundation of Basic Research Grant（18-29-23042）.

Corresponding author：QIU Han-xun，Associate professor. E-mail：hxqiu@usst.edu.cn

Author introduction：CHENG Lei，Master student. E-mail：ryoma0401@126.com

1 Introduction

As a novel type of energy storage devices, supercapacitors have been catching the eyes of scientific communities over the years owing to their distinguishing features of fast charging/discharging rate, long cycle life and high-power density[1,2]. According to the mechanisms of energy storage, electrochemical supercapacitors can be classified in the types of electrical double-layer capacitors (EDLCs) and pseudocapacitors. The EDLCs store energy by virtue of the adsorption of both cations and anions, whereas the pseudocapacitors via fast surface redox reactions of the electroactive materials[3,4]. It's well known that the electrode materials adopted intimately determine the performance of supercapacitors, which meets the demands for practical applications. Therefore, with the increasing desire for high performance supercapacitors, great efforts were devoted to improving and developing novel electrode materials in recent years[5-9]. It is strongly desired that a promising electrode material should possess such features as high electrical conductivity for rapid electron transfer, open hierarchical porous structure, superior wettability for the diffusion and access of electrolyte ions, low cost and availability.

Owing to its unique two-dimensional (2D) structure and outstanding mechanical, thermal, and electrical properties[10,11], graphene has been attracting tremendous attention since its discovery. Graphene-based hybrids have also been extensively studied because of the distinguished electrochemical performance presented when used as electrode materials of supercapacitors[12-16]. Especially hybrids with a three-dimensional (3D) structure achieved through a green hydrothermal process are more desirable than the basic 2D structured ones, due to the large specific surface area offered and the rapid access of electrolyte ions in the unique 3D graphene network. More studies have been therefore concentrated on 3D graphene-based hybrids recently, and considerable progresses have been consequently achieved[17-22].

As one of the important allotropes in carbon family, fullerene, typically C_{60}, has a cage structure consisting of pentagonal and hexagonal rings of carbon atoms. The particular structure of C_{60} makes it easy to interact with graphene by π-π conjugated system possessed by both C_{60} and graphene. Furthermore, C_{60} has exhibited lots of excellent properties, especially its good electrochemical performance[23,24]. On the other hand, the all-carbon hybrids or composites exhibits more advantages compared to those noble materials loaded graphene materials, ie. more light-weighted, less environmentally-consumed, more affordable, and easily fabricated[3-5,13,18]. Therefore, combining the advantages of two allotropes of carbon and developing a novel hybrid comprising all-carbon element are of great significance and interests. It was recently reported by Thirumalraj et al. that electrochemical reactive C_{60}-GO nanocomposite was synthesized by a simple sonication of C_{60} with a graphene oxide (GO) aqueous solution, and applied to the sensitive detection of dopamine[25]. And Yang et al reported the successful fabrication of reduced graphene oxide-wrapped fullerene wires via an assembly of reduced GO and fullerene by employing the liquid-liquid interfacial precipitation method[26]. Besides, a new strategy to combine C_{60} with graphene for the preparation of FA-GO-PEG/C_{60} nanohybrid was proposed by Hu et al by conjugating folic acid (FA) and polyethylene glycol (PEG) onto graphene oxide (GO) via an imide linkage for targeting phototherapy[27]. These researches are preferentially focusing on the potential applications of fullerene/graphene hybrids either in photovoltaics[28,29], the anti-corrosion and tribological properties of the polymer matrix[30,31]. Whereas the study on electrochemical performance of these hybrids working as electrode materials has been scarcely reported so far. Fortunately, Li-functionalized C_{60}/graphene composite employed as electrode materials in supercapacitors was reported recently, exhibiting a specific capacitance of 135.36 F g^{-1} at a current density of 1 A g^{-1}[32]. However, what this kind of hybrids performed is far from our expectation. It is therefore of significance to explore the promising electrochemical properties of fullerene/graphene hybrids and their potential applications in supercapacitors.

We are herein reporting the electrochemical performance of C_{60}/graphene hybrids that were achieved by combining C_{60} and graphene laminates via a facile hydrothermal process. It is worth noting that the all-carbon hybrid exhibits excellent electrochemical performance when used as electrode materials for supercapacitors, as is competitive to the reported graphene/metal oxides composites. This finding may broaden the way to developing promising all-carbon electrode materials for high performance supercapacitors.

2 Experimental

2.1 Reagents and materials

Fullerene (C_{60}, 99.99% purity) was commercially obtained from Fuller-Tech Co, Ltd. (Puyang, China). Graphite power, sodium nitrate ($NaNO_3$, AR), potassium permanganate ($KMnO_4$, AR), concentrated hydrochloric acid (HCl, AR), concentrated sulfuric acid (H_2SO_4, AR, 98%), hydrogen peroxide (H_2O_2, AR, 30%), were all purchased from Sinopharm Chemical Reagent (Shanghai, China). All of them were used as received unless otherwise stated. Deionized water (DI water) was used throughout the experiments.

2.2 Preparation of C_{60}/graphene hybrid

GO was synthesized from natural graphite via a modified Hummers method that was reported elsewhere[33-36]. It is worth noting that the obtained GO dispersion was freeze-dried to be solid prior to use in the following procedures. Series of concentrations ($mg \cdot mL^{-1}$) of homogeneous GO aqueous dispersion was obtained by ultrasonic dispersion of the as-obtained GO. C_{60}/graphene hybrid materials were synthesized in hydrothermal circumstances. Factors including the mass ratio of C_{60} to GO, hydrothermal temperature and reaction time have great influence on the structure of the hybrids and the electrochemical performance. A new thought of orthogonality experiments was therefore proposed and designed to optimize the experimental conditions in this study. Based on our previous study, three independent variables, the mass ratio of C_{60} to GO, temperature, and time involved in the hydrothermal process, were designated as A, B and C, respectively, which were considered as the key factors determining the structures and performance of the resulting materials. Their values were set to be 1∶6, 1∶8, 1∶10 for A, 120, 150, 180 ℃ for B, and 6, 9, 12, 15 h for C. With these parameters through orthogonal test methods, totally eighteen grouped experiments were carried out in the research (more information can be found in Table 1).

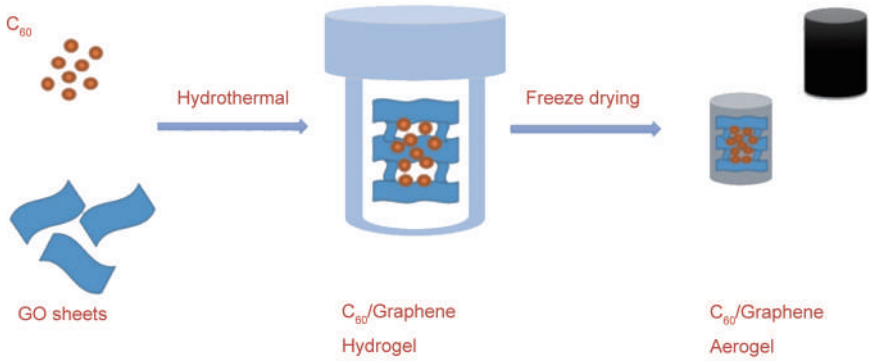

Fig. 1 Schematic illustration for preparation of C_{60}/graphene aerogels.

As for the procedures of performing experiments under the optimized conditions, 4.5 mg of C_{60} was dispersed into 5 mL of DI water with ultrasonication for 60 min, followed by mixing the dispersion with the aqueous solution of GO ($4.5\ mg \cdot mL^{-1}$, 8 mL), and stirring for 30 min so as to obtain a homogeneous mixture of C_{60} and GO. The mixture was subsequently contained in an autoclave that was heated to 150 ℃ and held for 12 h. After the reaction, the formed hydrogel was taken out and washed with DI water repeatedly until the complete removal of the excessive C_{60}. Finally, the 3D hierarchical porous structure of C_{60}/graphene aerogel was achieved via vacuum freeze-drying, designated as mC_{60}/graphene which exhibited the best electrochemical performance over all C_{60}/graphene hybrid materials prepared in this work. Experiment sets with different parameters were carried out in the same procedures as aforementioned. The schematic illustration for the preparation of C_{60}/graphene aerogels is shown in Fig. 1.

2.3 Characterization

Morphology and structure of samples were characterized by the following techniques. X-ray diffraction (XRD, Bruker D8-Advance) patterns were recorded for 2θ angles ranging from 5° to 70° to detect the crystal structure of samples. Morphology observation was conducted using a field-emission electron microscope (FESEM, accelerating voltage, 20 kV, beam current, 10 A, JEOL S-4800) by fixing specimens to the sample holder with a piece of adhesive carbon tape. Raman spectra were recorded using a Raman spectrometer (Horiba, LabRAM HR Evolution) equipped with a 532 nm Ar lines as the excitation source. Pore structure analysis was conducted by a physical adsorption instrument (Nitrogen adsorption – desorption, Micromeritics Instrument Ltd. ASAP 2020). X-ray photoelectron spectroscopy (XPS, ESCA PHI 5000/AXIS UltraDLD) was utilized to detect

the chemical bonds of samples.

2.4 Electrode preparation and electrochemical measurements

The electrochemical performance was carried out on a CHI760D electrochemical workstation using a three-electrode system, in which C_{60}/graphene served as the working electrode, platinum foil as the counter electrode, saturated calomel electrode as the reference electrode, and 6 mol/L potassium hydroxide (KOH) solution as the electrolyte. The working electrode was fabricated by the prepared aerogels without using any binder or conducting additives. A slice of the 3D columned aerogel was cut into 1 mm thickness and pressed onto a nickel foam sheet (1×1 cm^2) at 10 MPa for 30 s. The mass loading of the active material on each current collector was of 2 mg ± 0.5 mg. The cyclic voltammetry (CV) curves were performed at a voltage ranging from −1 and 0 V at scan rates of 10, 20, 50, 100 mV s^{-1}. The galvanostatic charging/discharging (GCD) tests were carried out at different current densities with a potential window ranging from −1 to 0 V. The electrochemical impedance spectrum (EIS) was recorded over the frequency ranging from 100 kHz to 0.01 Hz at open circuit potential with an AC voltage amplitude of 5 mV [37]. All electrochemical experiments were carried out at room temperature.

The gravimetric specific capacitances measured at a current density of 1 A g^{-1} were calculated based on GCD curves according to the following equation (1)[6],

$$C_g = \frac{I\Delta t}{\Delta V m} \tag{1}$$

where C_g is the gravimetric specific capacitance (F/g), I is the constant discharge current (A), Δt is the discharge time (s), ΔV is the range of charge voltage which is 1 V in this work, and m is the mass (g) of the active materials used for the fabrication of electrode.

The volumetric performance of a material was recently recommended as a more reliable parameter than gravimetric performance. Supercapacitors can be described by their volumetric specific capacitance, which can be expressed as follows[38]:

$$C_v = \rho C_g \tag{2}$$

Where C_v is the volumetric specific capacitance (F/cm^3), ρ is the particle density of active materials and C_g is the gravimetric specific capacitance (F/g) which can be calculated by Equation (1).

3 Results and discussion

3.1 Characterization of mC$_{60}$/graphene hybrids

Fig. 2 shows SEM images of rGO and mC$_{60}$/graphene aerogels at different magnifications. As shown distinctly, both graphene-based aerogels have a porous microstructure and comprise hierarchical pores with sizes ranging from nanometers to micrometers. By comparing the difference in microstructures, it can be easily found that the pores in mC$_{60}$/graphene are more orderly and hierarchical, and its size distribution is much narrower than rGO. The pore structure in mC$_{60}$/graphene is not only more diverse but also contains much thinner walls. Furthermore, the proportions of meso- and micropores in mC$_{60}$/graphene are much larger than the pure rGO aerogel in which macropores with micrometer sizes are dominant.

In order to further analyze the effect of C_{60} on the pore structure of mC$_{60}$/graphene, nitrogen isotherm adsorption and desorption experiments were performed on the samples. Fig. 3a shows the isothermal adsorption and desorption curves of nitrogen for rGO and mC$_{60}$/graphene aerogels. It can be seen that both the adsorption and desorption curves of rGO and mC$_{60}$/graphene are of hysteresis loops, and the adsorption and desorption behaviors belong to the type IV, indicating that mesoporous structures are presented in both rGO and mC$_{60}$/graphene samples. The non-closing of the hysteresis loops in the $0 < p/p_0 < 0.1$ low pressure region may be due to the irreversible adsorption of nitrogen. The BET surface area of C_{60}/graphene is 292.5 m$^2 \cdot$ g^{-1}, which is much larger than that of rGO. Fig. 3b shows the pore size distributions of rGO and C_{60}/graphene samples obtained by the density functional theory (DFT) algorithm. It can be found that the pores in mC$_{60}$/graphene are mostly distributed within 10 nm, indicating that micropores and small mesopores are dominant. This is quite different from those of rGO in which large mesopores and macropores account for a large proportion, as shown in the inset in the upper right corner of the figure presenting the pore size distribution curve from 0-200 nm. The pore size distribution of rGO is mainly concentrated in the macropore region of 50-150 nm. The discrepancy in pore structures of rGO and mC$_{60}$/graphene is definitely correlated with the addition of C_{60} during the construction of graphene- based aerogels. The introduction of C_{60} promotes the self-assembly to form a porous structure of graphene, favors the formation of micro- and mesopores, and optimizes the distribution of hierarchical pores during the hydrothermal self-assembly process, though the mechanism of C_{60} regulating the pore structure is under investigation yet. The pore size distribution is narrowed from the macropore region for rGO to the micro- and small mesopore region, which is in good accordance with the observation of SEM. It is well known that mesopores

in carbon-based electrode materials are responsible for the rapid ion-transportation with a minimized resistance, while micropores account for the enhancement of specific surface area, both of which are critical for electrode materials exhibiting better electrochemical performance of supercapacitors[39]. It is therefore believed that these significant differences in pore structure and distributions are attributed to the addition of C_{60} that may influence the assembly of graphene sheets and optimize the proportions of hierarchical pores during the formation of the aerogel in hydrothermal process. Besides, the addition of C_{60} promotes the electron transfer among the hierarchical pores, leading to the enhancement of electrochemical performance of the electrode materials. The rational construction of pores in mC_{60}/graphene sample make it promising in the use as electrode materials for high performance supercapacitors.

XRD patterns of C_{60}, rGO aerogel and mC_{60}/graphene hybrid were recorded to investigate the crystal structures of samples, as shown in Fig. 4a. Sharp peaks at $2\theta = 10.4°$, $17.4°$, $20.4°$ are typically observed for C_{60}. The pattern of rGO aerogel shows a broad peak located at around $2\theta = 25.7°$, attributed to (002) plane of graphite. Whereas for mC_{60}/graphene, characteristic peaks of both C_{60} and rGO aerogel are featured at about $10.8°$, $17.8°$, $20.8°$ and $26°$. The only difference lies in that the characteristic peaks of C_{60} are intensively depressed, as may be caused by the very small amount of C_{60} in the hybrid and the overlapping with the relatively strong broad peak of graphene. The evidence provided by XRD patterns indicates that C_{60} has been successfully doped into graphene laminates and formed a mC_{60}/graphene hybrid.

Raman spectra were conducted for distinguishing ordered and disordered crystal structures of carbon materials. Fig. 4b shows the Raman spectra of aerogels of rGO and mC_{60}/graphene. It can be seen that both spectra feature very strong *D*-band and *G*-band, typically originating from a breathing κ-point phonon with A_{1g} symmetry that is related to local defects and disorder, and the E_{2g} phonon of sp^2 hybridized carbon atom[40], respectively. Two strong peaks for rGO are located at around 1 347 and 1 586 cm^{-1}, while these for mC_{60}/graphene are

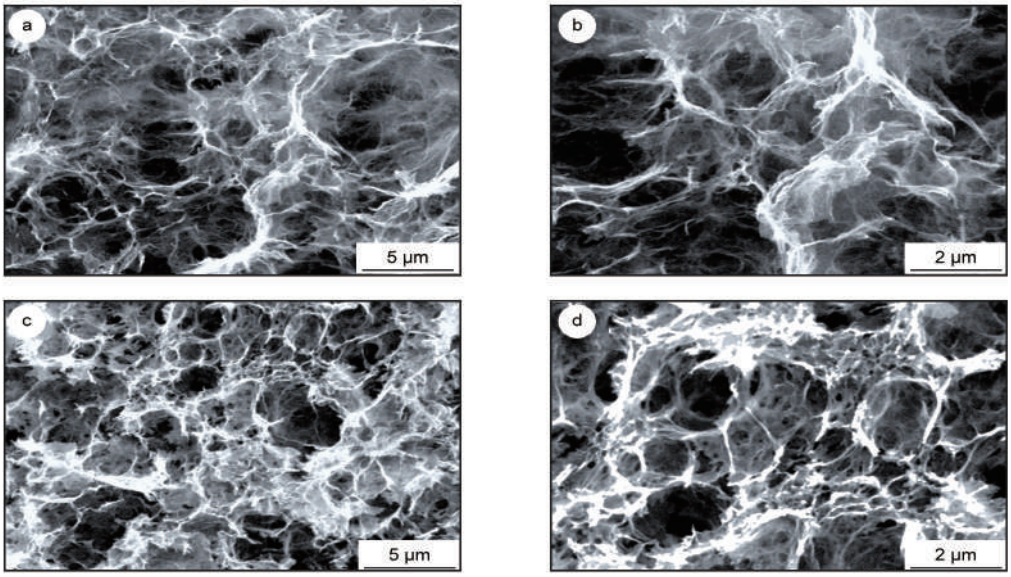

Fig. 2 SEM images of (a, b) rGO aerogel and (c, d) mC_{60}/graphene aerogel.

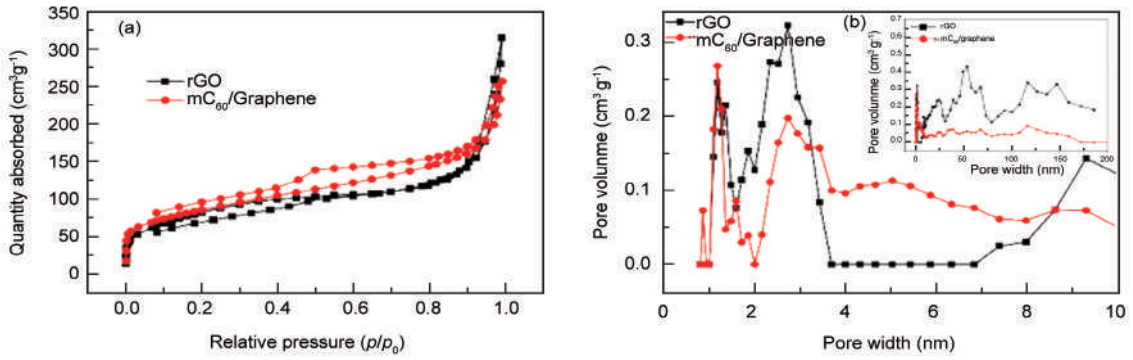

Fig. 3 (a) Nitrogen adsorption-desorption isothermal curves of rGO and mC_{60}/graphene and (b) their pore size distributions.

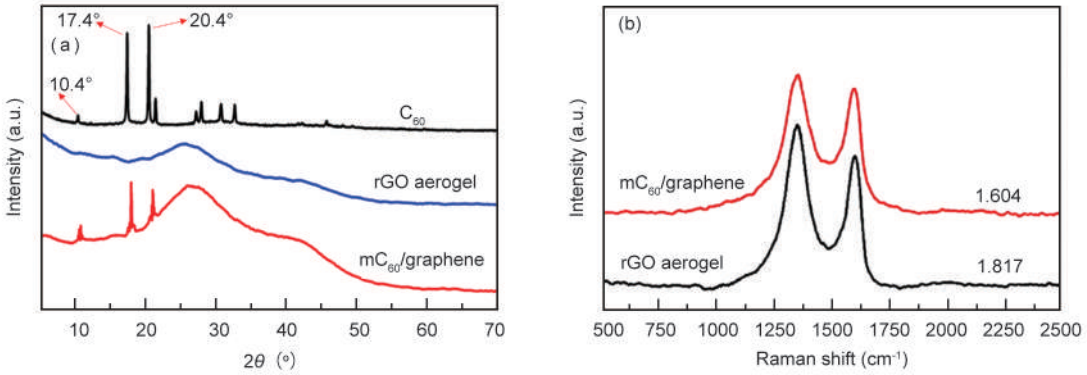

Fig. 4　(a) XRD patterns for C_{60}, rGO aerogel, and mC_{60}/graphene hybrid, (b) Raman spectra of rGO aerogel and mC_{60}/graphene hybrid.

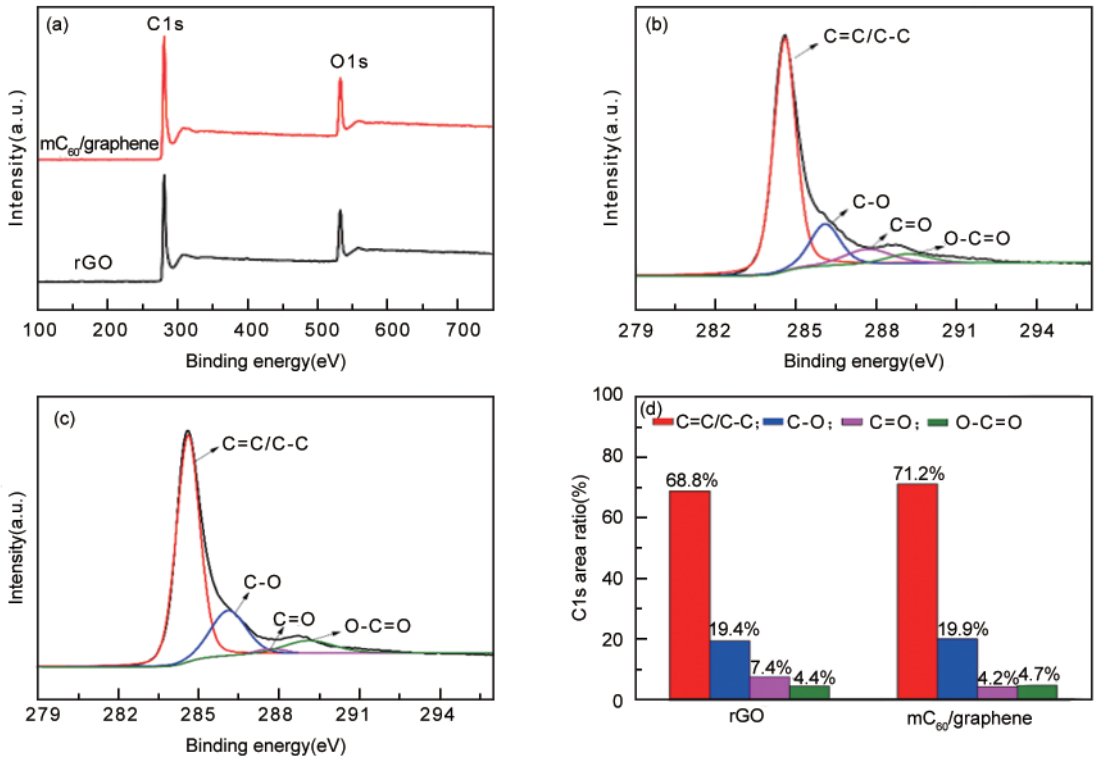

Fig. 5　(a) XPS spectra of rGO and mC_{60}/graphene, (b) C1s core-lever spectra of rGO and (c) mC_{60}/graphene, (d) the area ratios of four types of C in C1s peak in rGO and mC_{60}/graphene

centered at 1 349 and 1 589 cm^{-1}. The slight blue shifts of peaks for the hybrid imply an interaction between the C_{60} molecules and graphene laminates. A peak at about 1 465 cm^{-1} corresponding to the vibration of C_{60} is not found in the spectrum probably because its intensity is much weaker than the strong *D* band of graphene[41], so that is it is fully covered. The intensity ratio of *D* band to *G* band (I_D/I_G) has been extensively put forward as a useful indicator to evaluate the crystal structure of carbon materials[42]. Accordingly, the I_D/I_G ratio for graphene is 1.817, while for mC_{60}/graphene is 1.604. The slight decrease of I_D/I_G ratio in mC_{60}/graphene might be attributed to the less structure defects promoted by the presence of C_{60} in the hydrothermal process.

XPS spectra were conducted for the further analysis of the elemental composition and valence of samples. Fig. 5 shows XPS spectra of rGO and mC_{60}/graphene. As seen in Fig. 5a, both rGO and C_{60}/graphene exhibit C 1s peak near 285 eV and O 1s peak at 531 eV. Fig. 5b and 5c show the high resolution C 1s spectra of rGO and mC_{60}/graphene, respectively. The C 1s peak can be divided into four different types of C, which are C—C/C ═C at 284.6 eV, C—O at 286.1 eV, C ═O at 287.7 eV and O—C ═O at 289.1 eV. Fig. 5d shows the proportion of four dif-

ferent types of C in C 1s. By comparison, it is found that the intensity of the C ═O peak at 287.7 eV for mC_{60}/graphene is greatly weakened, indicating that the chemical bonds in graphene-based composites have been changed[43]. This may be due to the presence of the unique $sp^{2.8}$ hybrid structure of carbon atoms in C_{60} (i. e., between sp^2 hybrids and sp^3 hybrids). During the hydrothermal treatments, the strong π − π interaction between carbon hexagons in C_{60} and graphene skeletons affects the self-assembly of the 3D structure of graphene.

3.2 Electrochemical properties of C_{60}/graphene hybrid

The electrochemical performance of C_{60}/graphene as electrode materials for supercapacitors was evaluated by standard CV, GCD and EIS. Orthogonality experiments with the optimized conditions involving three independent variables, the mass ratio of C_{60} to GO (A), hydrothermal temperature (B), and reaction time (C), were systematically carried out, as shown in Table 1.

The data in Table 2 is the gravimetric specific capacitance of eighteen samples calculated by the Equation (1). As the results shown in Table 2, the optimized sample $A_2B_2C_3$ (mC_{60}/graphene) exhibits the maximum value of specific capacitance in all performed experiments. That is when the mass ratio of C_{60} to graphene is 1∶8 was employed and reaction was carried out at a hydrothermal temperature of 150 ℃ for 12 h, the hybrid with an optimized structure could be achieved, as accounted for the superior electrochemical performance of electrode materials for supercapacitors.

Fig. 6 presents CV curves of C_{60}/graphene electrode materials under different conditions. The CV curves of mC_{60}/graphene measured at a series of scan rates are shown in Fig. 6a. The relatively symmetric and rectangular shape of curves indicates that the electrode material behaves in a manner of EDLCs. Moreover, a pair of broad peaks are slightly observed especially with the increase of scan rates, as may be aroused by the presence of hydroxyl, carboxyl, and epoxyl functional groups in graphene sheets and C_{60} molecules. Therefore, mC_{60}/graphene exhibits characteristics of both EDLCs and pseudocapacitors. In addition, electrochemical dependence of the hybrids on the mass ratio, reaction time, and temperatures are demonstrated as well. For a better comparison, all of these curves were scanned at the same scan rate of 50 $mV \cdot s^{-1}$. Effects of the mass ratio A on CV curves were evaluated with hybrids that were prepared at 150 ℃ for 12 h (designated as AxB_2C_3 based on Table 1, where variable X represents the mass ratio), as shown in Fig. 6b. Similarly, dependences of CV on reaction time C and temperature B were illustrated by samples of A_2B_2Cx and A_2BxC_3 in Fig. 6c and d, respectively. By comparing the curves, it is easily found that sample mC_{60}/graphene ($A_2B_2C_3$) exhibits the largest area of CV curve among all the electrodes materials, suggesting the optimized experimental conditions and consequently a best capacitance enhancement due to the addition of C_{60}.

GCD curves of rGO and C_{60}/graphene electrode materials under different conditions are presented in Fig. 7. The curves of pure rGO and C_{60}/graphene AxB_2C_3 with a series mass ratio of C_{60} to GO (1∶6 & 1∶8&1∶10) were tested at a current density of 1 $A \cdot g^{-1}$, as shown in Fig. 7a. It can be seen that no matter what the mass ratio is, the hybrids exhibit much better charging/discharging performance than the pure rGO material. Moreover, when the mass ratio of C_{60} to GO reaches 1∶8, the hybrid behaves the optimized GCD performance, and its specific capacitances calculated based the equation (1) is up to 332.3 $F \cdot g^{-1}$ at 1 $A \cdot g^{-1}$ that is enhanced by 54.5% in contrast to 215.1 $F \cdot g^{-1}$ for the pure rGO. This value is twofold

Table 1 The setting of the experimental parameters.

Level	Ratio(A)	Temperature(B)/℃	Time(C)/h
1	1∶6	120	6
2	1∶8	150	9
3	1∶10	180	12
4	–	–	15

Table 2 Specific capacitance of samples at a current density of 1 $A \cdot g^{-1}$ (Sample ID is derived from Table 1).

	ID	$A_1B_1C_1$	$A_1B_2C_2$	$A_1B_3C_3$	$A_2B_2C_3$	$A_2B_3C_1$	$A_2B_1C_2$
C(F/G)		222.9	223.8	244.6	332.3	272.4	234.6
	ID	$A_3B_3C_2$	$A_3B_1C_3$	$A_3B_2C_1$	$A_1B_1C_2$	$A_1B_2C_3$	$A_1B_3C_4$
C(F/G)		279.7	238.6	228.7	235.2	263.8	239.8
	ID	$A_2B_2C_4$	$A_2B_3C_2$	$A_2B_1C_3$	$A_3B_3C_3$	$A_3B_1C_4$	$A_3B_2C_2$
C(F/G)		294.2	296.5	254.8	230.8	253.8	232.4

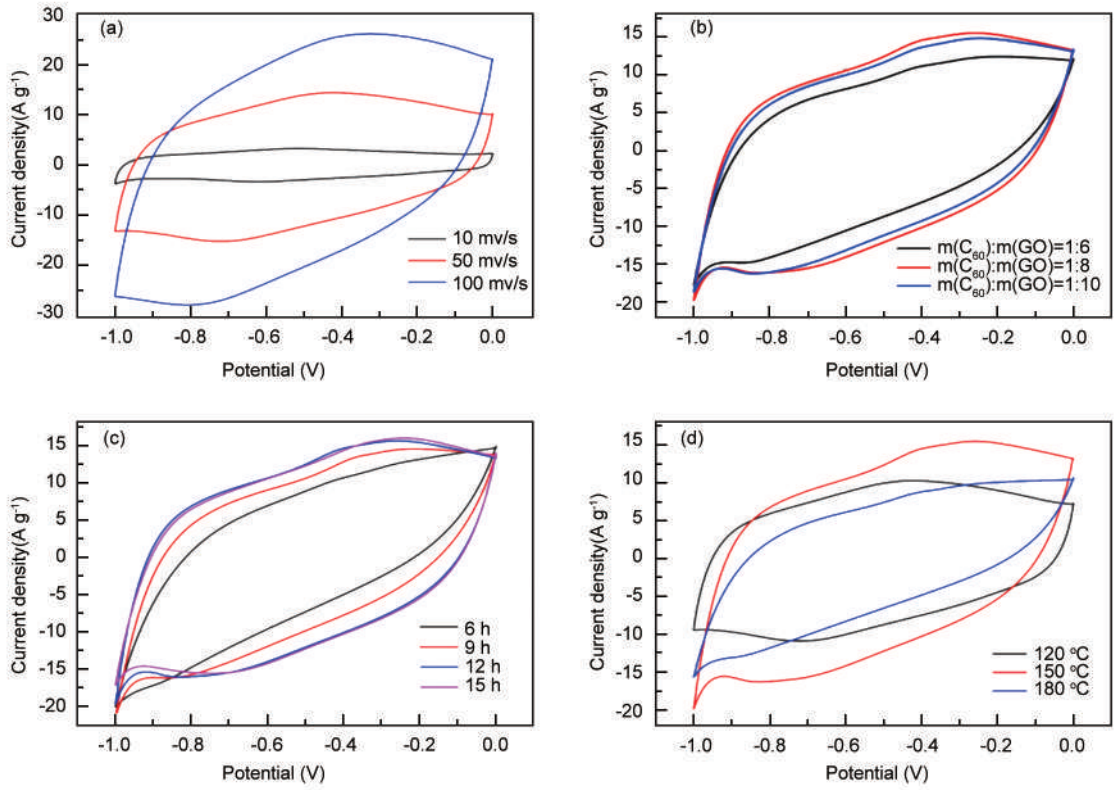

Fig. 6　(a) CV curves of mC_{60}/graphene hybrid at various scan rates, effects of (b) the mass ratio, (c) reaction time and (d) temperature on CV curves of as-prepared samples measured at the scan rate of 50 $mV \cdot s^{-1}$.

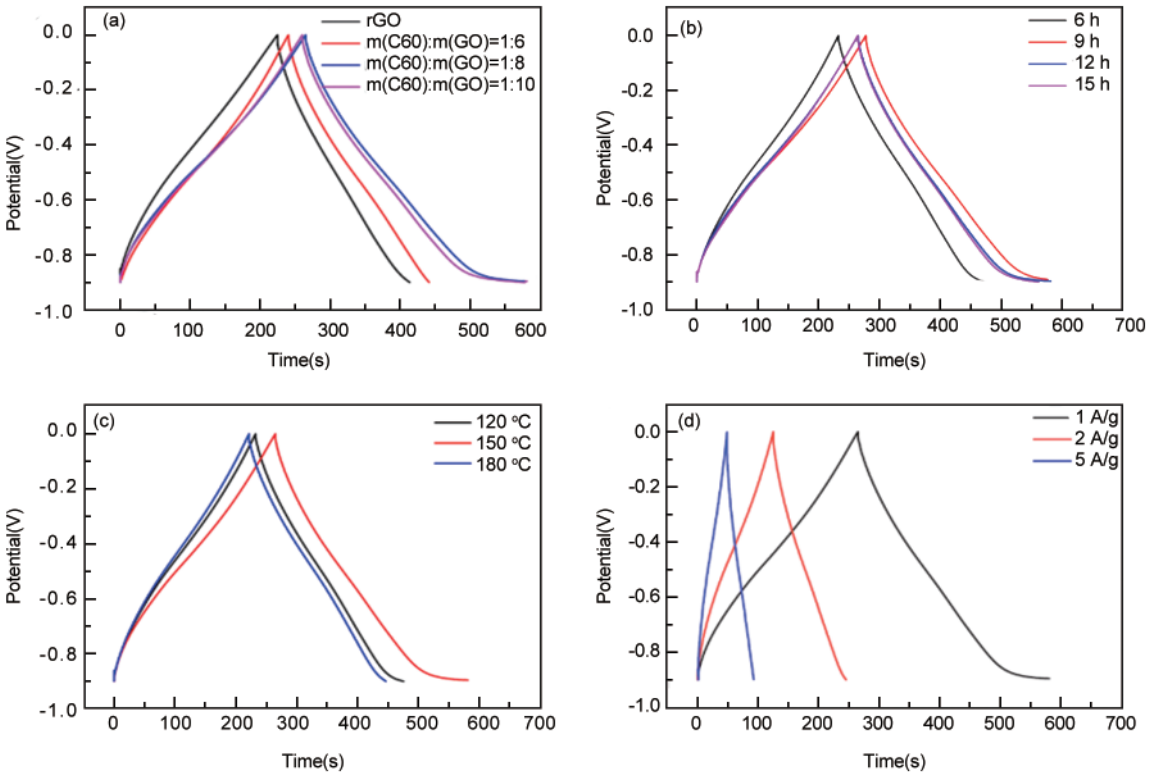

Fig. 7　GCD curves of pure rGO and C_{60}/graphene samples demonstrating effects of (a) the mass ratio, (b) reaction time, (c) temperature on electrochemical behaviors and (d) GCD curves of mC_{60}/graphene at different current densities. Note that GCD curves in Fig. 7(a), (b) and (c) were tested at the current density of 1 $A \cdot g^{-1}$.

higher than the similar work in which Li-functionalized C_{60}/graphene was used as electrode materials for supercapacitors, exhibiting a specific capacitance of 135.36 $F \cdot g^{-1}$ at 1 A g^{-1} [32]. The increased capacitance for C_{60}/graphene hybrid electrode can be attributed to the intercalation of an appropriate amount of C_{60} into graphene laminates, which favored the formation of an optimal porous structure of hybrids. When the excessive C_{60} was doped to graphene however, aggregation of C_{60} may occur, thus lowering the synergistic effect between fullerene and graphene. Fig. 7b remarks the difference in GCD curves of C_{60}/graphene $A_2B_2C_x$ that were prepared with the mass ratio of 1∶8 and at 150 ℃ for a series of reaction time, demonstrating that samples with better GCD performance could be achieved as long as the reaction time exceeds 12 h. Fig. 7c shows the GCD curves of C_{60}/graphene $A_2B_xC_3$ that were prepared with the mass ratios of 1∶8 and at a series of reaction temperatures for 12 h. It can be calculated that the specific capacitance reaches a maximum value when the temperature of 150 ℃ is employed. Comparatively the specific capacitances are 277.2 $F \cdot g^{-1}$ at 180 ℃ and 254.8 $F \cdot g^{-1}$ at 120 ℃. This may be due to the effect of the degree of hydrothermal reduction. The lower temperature and the weaker reducing ability will make the three-dimensional structure of the sample unstable. When the temperature is up to 180 °C, with the increasing of reduction degree of GO, the distance between the layers will be stacked closer, and the agglomeration becomes serious, therefore the mesopore size becomes smaller. Therefore, the experimental conditions under which samples exhibiting the optimal electrochemical performance can be obtained. Fig. 7d exhibits the GCD curves of mC60/graphene that were tested at different current densities (332.3 $F \cdot g^{-1}$ at 1 $A \cdot g^{-1}$, 263.8 $F \cdot g^{-1}$ at 2 $A \cdot g^{-1}$, 241.1 $F \cdot g^{-1}$ at 5 $A \cdot g^{-1}$). Similarly as reported previously, with increasing the current density, the electrochemical performance may decrease slightly. Nevertheless mC_{60}/graphene behaves as an excellent electrode material, which is superior to the pure rGO.

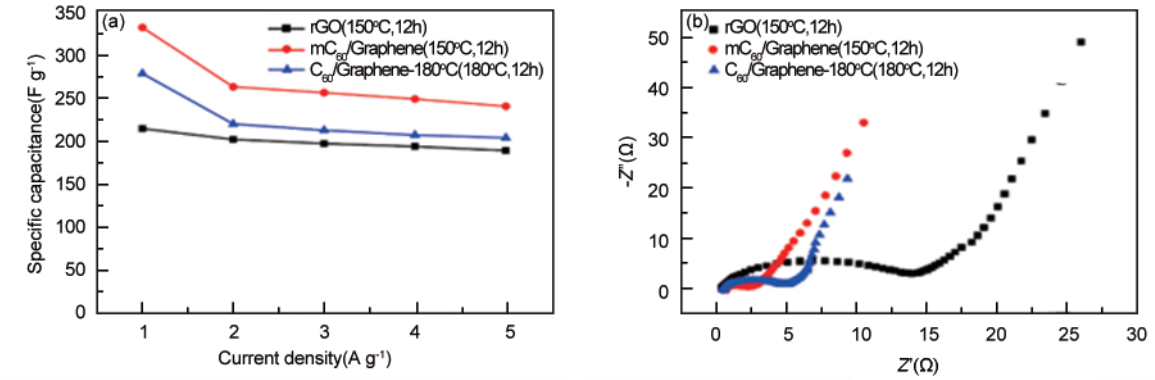

Fig. 8 (a) Specific capacitance at different current densities and (b) Nyquist plots of the electrodes based on rGO, mC_{60}/graphene and C_{60}/graphene.

Fig. 8(a) presents the specific capacitance of samples measured at a series of current densities, which are calculated based on GCD curves in Fig. 7. By comparison, no matter what current density was employed in the electrochemical test, mC_{60}/graphene electrode material always exhibits much higher specific capacitance than those unoptimized hybrids and the pure rGO, although the specific capacitance of mC_{60}/graphene decreases slightly with the increase of the current density as usual. The enhanced capacitance is coincident with CV results aforementioned. Moreover, mC_{60}/graphene exhibited a high volumetric capacitance of 200.9 $F \cdot cm^{-3}$ with a density of ~ 0.6 $g \cdot cm^{-3}$. EIS is an effective method to measure the internal resistance and charge transfer kinetics of electrode materials. In Fig. 8(b), Nyquist plots of the electrodes based on rGO, C_{60}/graphene and mC_{60}/graphene were conducted in a 6 mol/L KOH solution at the frequency range of 100 kHz to 0.01 Hz. In general, a Nyquist plot includes a semicircle in a high frequency region and a straight line in a low frequency region. The high frequency region is correlated to charge transfer resistance and the low frequency region to capacitive performance. As shown in Fig. 8(b), in the high frequency, the semicircle diameters of mC_{60}/graphene and C_{60}/graphene-180 (1∶8; 180 ℃; 12 h) hybrid are remarkably smaller than that of the pure rGO, indicating that the introduction of C_{60} to rGO has significantly enhanced the conductive behavior of electrodes. This could be ascribed to the excellent electron accepting ability of C_{60} that may promote the ultrafast electron transfer among graphene oxide sheets. Furthermore, in the low frequency, mC_{60}/graphene exhibits a vertical curve with a relatively large slope,

suggesting an enhanced capacitive performance. Through the EIS measurements, it can be concluded that the introduction of C_{60} into rGO laminates accounts for the enhancement in capacitance performance of mC_{60}/graphene hybrids, typically i. e. the lower internal resistance, better charge transfer and ionic conductivity.

The measurements of CV, GCD, and EIS have evidenced that C_{60}/graphene hybrids possess excellent electrochemical properties and performance as promising electrode materials for high performance supercapacitors. The enhancement of electrochemical performance is definitely attributed to the hierarchically porous structure of C_{60}/graphene hybrids. It is elucidated that the presence of C_{60} favored the self – assembly of the 3D structure of C_{60}/graphene under high pressure hydrothermal conditions via strong π-π interaction between hexagons in C_{60} and graphene skeletons. Moreover, the attached C_{60} molecules endowed the hybrids with an optimized porous microstructure and more redox-active sites, contributing to the remarkably enhanced electrochemical performance when the hybrids were tested as electrodes for supercapacitors.

Table 3　Comparison of representative specific capacitance of all-carbon and non-all-carbon electrodes.

Raw materials	Current density ($A\ g^{-1}$)	Specific capacitances ($F\ g^{-1}$)	Application	Ref.
This work	1	332.3	All-carbon SC	
C_{60}/graphene	1	136.4	All-carbon SC	[32]
Porous carbon /CNT/graphene	1	175.6	All-carbon SC	[44]
CNT/graphene	1	322	All-carbon SC	[45]
Porous core-shell carbon fibers	0.5	98	All-carbon SC	[46]
GO/PG	0.2	120	All-carbon SC	[47]
AC/CNT	1	297.9	All-carbon SC	[48]
PANI/graphene	2.22	824	Non-all--carbon SC	[49]
N-graphene	1	210	Non-all--carbon SC	[50]
Sn-Mn_3O_4/C	1	222	Non-all--carbon SC	[51]
rGO/RuO_2	1	343	Non-all--carbon SC	[52]
N-AC	0.4	185	Non-all--carbon SC	[53]
N-graphene/CNT	0.5	180	Non-all--carbon SC	[54]
NS-graphene	1	309	Non-all--carbon SC	[55]
BNP-rGO	1	350	Non-all--carbon SC	[56]

The capacitance performance of the C_{60}/graphene electrode prepared in this work (332.3 $F\cdot g^{-1}$ at 1 $A\cdot g^{-1}$) is superior to almost all previously reported all-carbon electrode-based supercapacitors, and even competitive to some of non-full-carbon electrodes. The synergistic effects from the different forms of nanocarbons included in this reported all-carbon hybrid, namely the 0D fullerene, and 2D GO, as well as the formed hierarchical porous structure, render the hybrid outstanding capacitance performance. This finding presents a promising all-carbon based electrode material for fabricating high performance supercapacitors in future.

4　Conclusions

This work demonstrated a facile fabrication of 3D hierarchical porous structured all-carbon hybrids (C_{60}/graphene) employed as competitive electrodes for high performance supercapacitors. The C_{60}/graphene hybrids were achieved via a facile hydrothermal method. It is elucidated that the mass ratio of C_{60} to graphene, reaction time and temperature were key factors determining the porous structure and electrochemical properties of hybrids. By introducing C_{60} molecules into graphene laminates, the specific capacitance of C_{60}/graphene was considerably enhanced. Typically, when the mass ratio of C_{60} to GO is 1∶8, and the hydrothermal time and temperature are 12 h and 150 ℃, respectively, the specific capacitance of mC_{60}/graphene hybrid can reach 332.3 $F\cdot g^{-1}$, which is enhanced by 54.5% as compared with the pure rGO (215.1 $F\cdot g^{-1}$) at the same current density of 1 $A\cdot g^{-1}$. The enhancement could be ascribed to the synergistic effect rising from the hybridization of fullerene and graphene which favors the self-assembly of the hierarchical porous structure of mC_{60}/graphene under high pressure hydrothermal conditions via the π-π interaction between carbon hexagons of C_{60} and graphene skeletons. The capacitance performance of hybrids prepared in this work is comparative and superior to those of presentative carbon-based electrode devices reported previously. This finding therefore shed valuable light for the future design and preparation of all-carbon materials for the use as electrodes of highly performed energy storage devices.

References

[1] González A, Goikolea E, Barrena J A, et al. Review on supercapacitors: Technologies and materials [J]. Renewable & Sus-

tainable Energy Reviews, 2016, 58: 1189-1206.
[2] Jiang H, Lee P S, Li C. 3D carbon based nanostructures for advanced supercapacitors [J]. Energy & Environmental Science, 2013, 6(1): 41-53.
[3] Annamalai K P, Zheng X, Gao J, et al. Nanoporous ruthenium and manganese oxide nanoparticles/reduced graphene oxide for high – energy symmetric supercapacitors [J]. Carbon, 2019, 144: 185-192.
[4] Jiao C, Zhang W, Su F, et al. Research progress on electrode materials and electrolytes for supercapacitors [J]. New Carbon Materials, 2017, 32 (2): 106-115.
[5] Farbod F, Mazloum-Ardakani M, Naderi H R, et al. Synthesis of a porous interconnected nitrogen-doped graphene aerogel matrix incorporated with ytterbium oxide nanoparticles and its application in superior symmetric supercapacitors [J]. Electrochimica Acta, 2019, 306: 480-488.
[6] Qiu H X, Han X B, Qiu F L, et al. Facile route to covalently-jointed graphene/polyaniline composite and it's enhanced electrochemical performances for supercapacitors [J]. Applied Surface Science, 2016, 376: 261-268.
[7] Yang W, Hou L Q, Xu X W, et al. Carbon nitride template – directed fabrication of nitrogen-rich porous graphene-like carbon for high performance supercapacitors [J]. Carbon, 2018, 130: 325-332.
[8] Kovalska E, Kocabas C. Organic electrolytes for graphene – based supercapacitor: Liquid, gel or solid [J]. Materials Today Communications, 2016, 7: 155-160
[9] Guo W, Yu C, Li S, et al. High-stacking-density, superior-roughness LDH bridged with vertically aligned graphene for high-performance asymmetric supercapacitors [J]. Small, 2017, 13(37): 1288.
[10] Huang X, Qi X Y, Boey F, et al. Graphene-based composites [J]. Chemical Society Reviews, 2012, 41(2): 666-686.
[11] Zhu Y W, Murali S, Cai W W, et al. Graphene and graphene oxide: synthesis, properties, and applications [J]. Advanced Materials, 2010, 22(46): 3906-3924.
[12] Xie B H, Wang Y, Lai W H, et al. Laser-processed graphene based micro-supercapacitors for ultrathin, rollable, compact and designable energy storage components [J]. Nano Energy, 2016, 26: 276-285.
[13] Su F Y, Xie L J, Sun G H, et al. Theoretical research progress on the use of graphene in different electrochemical processes [J]. Carbon, 2016, 110: 521.
[14] Tan M, Zheng J, Li P, et al. Preparation and modification of high performance porous carbons from petroleum coke for use as supercapacitor electrodes [J]. New Carbon Materials, 2018, 31: 343-351.
[15] Qi K, Hou R Z, Zaman S, et al. A Core/shell structured tubular graphene nanoflakes-coated polypyrrole hybrid for all-solid-state flexible supercapacitor [J]. Journal of Materials Chemistry A, 2018, 6(9): 3913-3918.
[16] Chen L, Li D P, Chen L, et al. Core-shell structured carbon nanofibers yarn@ polypyrrole@ graphene for high performance all-solid-state fiber supercapacitors [J]. Carbon, 2018, 138: 264-270.
[17] Jha P K, Gupta K, Debnath A K, et al. 3D mesoporous reduced graphene oxide with remarkable supercapacitive performance [J]. Carbon, 2019, 148: 354-360.
[18] Yuan J J, Zhu J W, Bi H P, et al. Graphene-based 3D composite hydrogel by anchoring Co_3O_4 nanoparticles with enhanced electrochemical properties [J]. Physical Chemistry Chemical Physics, 2013, 15(31): 12940-12945.
[19] Wei F, Zhang H F, He X J, et al. Synthesis of porous carbons from coal tar pitch for high-performance supercapacitors [J]. New Carbon Materials, 2019, 34(2): 132-139.
[20] Zhang Q Q, Wang Y, Zhang B Q, et al. 3D superelastic graphene aerogel-nanosheet hybrid hierarchical nanostructures as high-performance supercapacitor electrodes [J]. Carbon, 2018, 127: 449-458.
[21] Su X L, Fu L, Cheng M Y, et al. 3D nitrogen-doped graphene aerogel nanomesh: Facile synthesis and electrochemical properties as the electrode materials for supercapacitors [J]. Applied Surface Science, 2017, 426: 924-932.
[22] Caliman C C, Mesquita A, Cipriano D F, et al. One-pot synthesis of amine-functionalized graphene oxide by microwave-assisted reactions: An outstanding alternative for supporting materials in supercapacitors [J]. RSC Advances, 2018, 8(11): 6136-6145.
[23] Shrestha L K, Yamauchi Y, Hill J P, et al. Fullerene crystals with bimodal pore architectures [J]. Journal of American Chemical Society, 2013, 135: 586-589.
[24] Shrestha L K, Ji Q M, Mori T, et al. Fullerene nanoarchitectonics: From zero to higher dimensions [J]. Chemistry-An Asian Journal, 2013, 8(8): 1662-1679.
[25] Thirumalraj B, Palanisamy S, Chen S M, et al. Preparation of highly stable fullerene C_{60} decorated graphene oxide nanocomposite and its sensitive electrochemical detection of dopamine in rat brain and pharmaceutical samples [J]. Journal of Colloid & Interface Science, 2015, 462: 375-381.
[26] Yang J, Heo M, Lee H J, et al. Reduced graphene oxide (rGO)-wrapped fullerene (C_{60}) wires [J]. ASC Nano, 2011, 5(10): 8365-8371.
[27] Hu Z, Li J, Huang Y D, Chen L, et al. Functionalized graphene/C_{60} nanohybrid for targeting photothermally enhanced photodynamic therapy [J]. RSC Advances, 2014, 5(1): 654-664.
[28] Kim K, Lee T H, Santos E J, et al. Structural and electrical investigation of C_{60}-graphene vertical heterostructures [J]. ACS Nano, 2015, 9(6): 5922-5928.
[29] Zhang X Y, Huang Y, Wang Y, et al. Synthesis and characterization of a graphene-C_{60} hybrid material [J]. Carbon, 2009, 47(1): 334-337.
[30] Mo M T, Zhao W J, Chen Z F, et al. Excellent tribological and anti-corrosion performance of polyurethane composite coatings reinforced with functionalized graphene and graphene oxide nanosheets [J]. RSC Advances, 2015, 5(70): 56486-56497.
[31] Huh J H, Kim S H, Chu J H, et al. Enhancement of seawater corrosion resistance in copper using acetone – derived graphene coating [J]. Nanoscale, 2014, 6(8): 4379-4386.
[32] Ma J, Guo Q, Gao H L, et al. Synthesis of C_{60}/graphene composite as electrode in supercapacitors [J]. Fullerenes Nanotubes and Carbon Nanostructures, 2015, 23(6): 477-482.
[33] Li H L, Dai S C, Miao J, et al. Enhanced thermal conductivity of graphene/polyimide hybrid film via a novel "molecular welding" strategy [J]. Carbon, 2018, 126: 319-327.
[34] Qiu H X, Qiu F L, Han X B, et al. Microwave – irradiated

preparation of reduced graphene oxide-Ni nanostructures and their enhanced performance for catalytic reduction of 4-nitrophenol [J]. Applied Surface Science, 2017, 407: 509-517.

[35] Qiu H X, Han X B, Li J, et al. Microwave involved synthesis of graphene/polyaniline nanocomposite with superior electrochemical performance [J]. Journal of Nano Research, 2017, 46: 212-224.

[36] Yang Z Z, Zheng Q B, Qiu H X, et al. A simple method for the reduction of graphene oxide by sodium borohydride with $CaCl_2$ as a catalyst [J]. New Carbon Materials, 2015, 30(1): 41-47.

[37] Gui D Y, Liu C L, Chen F Y, et al. Preparation of polyaniline/graphene oxide nanocomposite for the application of supercapacitor [J]. Applied Surface Science, 2014, 307: 172-177.

[38] Wang Q, Yan J, Fan Z J. Carbon materials for high volumetric performance supercapacitors: Design, progress, challenges and opportunities [J]. Energy Environmental Science, 2016, 9(3): 729-762.

[39] Yao L, Yang G Z, Han P, et al. Three-dimensional beehive-like hierarchical porous polyacrylonitrile – based carbons as a high performance supercapacitor electrodes [J]. Journal of Power Sources, 2016, 315: 209-217.

[40] Hasdeo E H, Nugraha A R T, Dresselhaus M S, et al. Fermi energy dependence of first-and second-order Raman spectra in graphene: Kohn anomaly and quantum interference effect [J]. Physical Review B, 2016, 94(7): 075104.

[41] Qiu H X, Shi Z J, Zhang S L, et al. Synthesis and Raman scattering study of double-walled carbon nanotube peapods [J]. Solid State Communications, 2006, 137(12): 654-657.

[42] Stankovich S, Dikin D A, Piner R D, et al. Synthesis of graphene-based nanosheets via chemical reduction of exfoliated graphite oxide [J]. Carbon, 2007, 45(7): 1558-1565.

[43] Spyrou K, Kang L, Diamanti E K, et al. A novel route towards high quality fullerene-pillared graphene [J]. Carbon, 2013, 61: 313-320.

[44] You B, Jiang J, Fan S. Three-Dimensional Hierarchically Porous All-Carbon Foams for Supercapacitor [J]. ACS Applied Materials & Interfaces, 2014, 6(17): 15302-15308.

[45] Wang C, Liu D, Chen S, et al. All-carbon ultrafast supercapacitor by integrating multidimensional nanocarbons [J]. Small, 2016, 12(41): 5684-5691.

[46] Zhou W J, Zhou K, Liu X J, et al. Flexible wire-like all-carbon supercapacitors based on porous core-shell carbon fibers [J]. Journal of Materials Chemistry A, 2014, 2(20): 7250-7255.

[47] Du W C, Qi S P, Zhou B, et al. A surfactant-free water-processable all-carbon composite and its application to supercapacitor [J]. Electrochim Acta, 2014, 146: 353-358.

[48] Xu G H, Zheng C, Zhang Q, et al. Binder-free activated carbon/carbon nanotube paper electrodes for use in supercapacitors [J]. Nano Research, 2011, 4(9): 870-881.

[49] Wu J F, Zhang Q E, Wang J J, et al. A self-assembly route to porous polyaniline/reduced graphene oxide composite materials with molecular-level uniformity for high-performance supercapacitors [J]. Energy & Environmental Science, 2018, 11(5): 1280-1286.

[50] Haque E, Islam M M, Pourazadi E, et al. Nitrogen doped graphene via thermal treatment of composite solid precursors as a high performance supercapacitor [J]. RSC Advances, 2015, 5(39): 30679-30686.

[51] Zhao Y F, Ran W, Xiong D B, et al. Synthesis of Sn-doped Mn_3O_4/C nanocomposites as supercapacitor electrodes with remarkable capacity retention [J]. Materials Letters, 2014, 118: 80-83.

[52] Zhang J, Jiang J, Li H, et al. A high-performance asymmetric supercapacitor fabricated with graphene-based electrodes [J]. Energy& Environmental Science, 2011, 4(10): 4009-4015.

[53] Li B, Dai F, Xiao Q F, et al. Nitrogen-doped activated carbon for a high energy hybrid supercapacitor [J]. Energy& Environmental Science, 2016, 9(1): 102-106.

[54] You B, Wang L L, Yao L, et al. Three dimensional N-doped graphene-CNT networks for supercapacitor [J]. Chemical Communications, 2013, 49(44): 5016-5018.

[55] Wu D, Wang T, Wang L, et al. Hydrothermal synthesis of nitrogen, sulfur co-doped graphene and its high performance in supercapacitor and oxygen reduction reaction [J]. Microporous and Mesoporous Materials, 2019, 290: 109556.

[56] Pan Z H, Zhi H Z, Qiu Y C, et al. Achieving commercial-level mass loading in ternary-doped holey graphene hydrogel electrodes for ultrahigh energy density supercapacitors [J]. Nano Energy, 2018, 46: 266-276.